THE JOURNAL OF PHYSICAL CHEMISTRY A
A JOURNAL OF THE AMERICAN CHEMICAL SOCIETY

pubs.acs.org/JPCA Article

Inferring the Energetics of CO_2−Aniline Adduct Formation from Vibrational Spectroscopy

Berk Delibas, Kareesa J. Kron, Daniel E. Cotton, Noemi Salazar, Shaama Mallikarjun Sharada,* and Jahan M. Dawlaty*

Cite This: *J. Phys. Chem. A* 2023, 127, 5162−5170 Read Online

ABSTRACT: Control of atmospheric CO_2 is an important contemporary scientific and engineering challenge. Toward this goal, the reaction of CO_2 with amines to form carbamate bonds is an established method for CO_2 capture. However, controllable reversal of this reaction remains difficult and requires tuning the energetics of the carbamate bond. Through IR spectroscopy, we show that a characteristic frequency observed upon carbamate formation varies as a function of the substituent's Hammett parameter for a family of *para*-substituted anilines. We present computational evidence that the vibrational frequency of the adducted CO_2 serves as a predictor of the energy of formation of the carbamate. Electron donating groups typically enhance the driving force of carbamate formation by transferring more charge to the adducted CO_2 and thus increasing the occupancy of the antibonding orbital in the carbon−oxygen bonds. Increased occupancy of the antibonding orbital within adducted CO_2 indicates a weaker bond, leading to a red-shift in the characteristic carbamate frequency. Our work serves the large field of CO_2 capture research where spectroscopic observables, such as IR frequencies, are more easily obtainable and can stand in as a descriptor of driving forces.

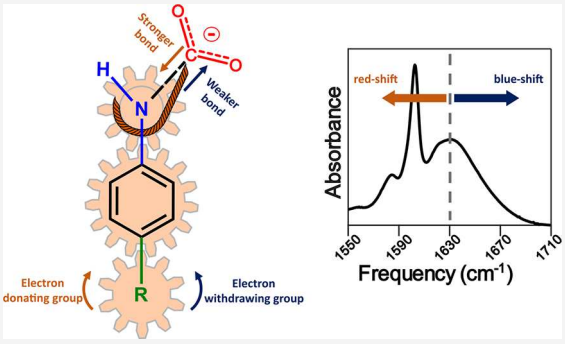

■ INTRODUCTION

Contemporary climate models project that we must not only eliminate current emissions but also perform direct-air capture to lower atmospheric CO_2 concentrations.[1] The past decade has seen an increase in scientific and engineering focus on improved and new methods for CO_2 capture.[2−5] Such approaches can be broadly categorized as irreversible and reversible methods. In the former, CO_2 irreversibly reacts with an absorber, for example with calcium ions, to form insoluble carbonaceous materials.[6−10] Examples of reversible CO_2 capture include temperature, pressure, and pH swings where thermodynamic parameters of the system are modulated to control the CO_2 equilibria.[6,7,11,12] Such approaches are often energy-intensive, expensive, environmentally hazardous, and not modular.

Organic Lewis bases, such as amines, offer chemical tunability and versatility for CO_2 capture. In these systems, the lone pair of the amine forms a Lewis adduct with the carbon of CO_2 to make a carbamate bond. Reaction of CO_2 with alkylamines like monoethanolamine are the prototype of this class and have been extensively studied.[6,13−16] To achieve better reversibility, sp^2 nitrogen centers have been proposed a as a viable approach.[17] Despite the rich literature on organic amines, understanding their reaction mechanisms with CO_2 remains a challenge.[18,19] For an ideal reversible CO_2 capture system, the strength of interaction between CO_2 and the capturing agent must simultaneously be strong enough to drive efficient absorption and weak enough to induce easy desorption.[11,20] Therefore, engineering the molecular details of CO_2 binding is critical.

In this work, we use aniline as a modular platform to systematically explore the energetics of CO_2 absorption (Figure 1).[18] We show that by adding various substituents to the aniline core, the carbamate reaction energy can be tuned. The substituents' electron donating/withdrawing ability is quantitatively represented by their Hammett parameters, σ_p.[21−23] Other studies have shown the aniline−CO_2 equilibrium depends on σ_p[18] and that the Hammett parameter correlates well with the pK_a of aniline derivatives.[24] Moreover, as some of us have previously shown,[22] this has some similarities to the polarization that an electrode induces on an adsorbed molecule. Therefore, trends seen in bulk measurements of functionalized anilines may be translated to an electrode surface for a reversible carbon capture system.

Received: February 28, 2023
Revised: May 22, 2023
Published: June 8, 2023

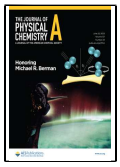

https://doi.org/10.1021/acs.jpca.3c01406
J. Phys. Chem. A 2023, 127, 5162−5170

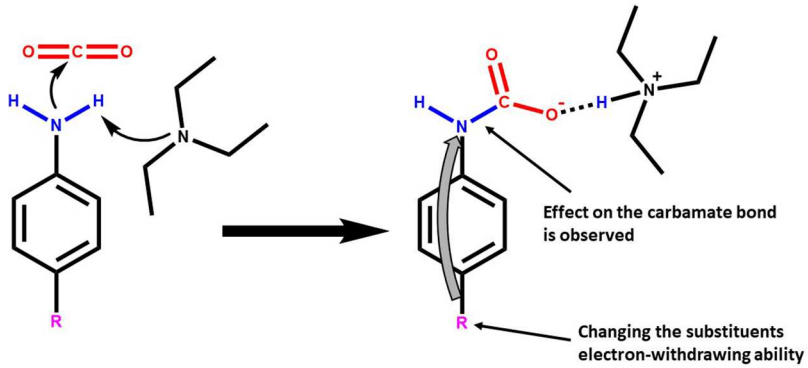

Figure 1. Reaction of *para*-substituted aniline with CO_2 in the presence of triethylamine.

Through a combination of computational and experimental work, we identify that the vibrational frequency of the adducted CO_2 serves as a convenient observable for the bond strength of the formed carbamates. The ability to use vibrational frequency to predict reaction energy is valuable due to the difficulties of performing calorimetry or precise measurement of equilibrium constants in many practical applications.

Tassaing and co-workers have previously studied the interaction of a series of substituted anilines with supercritical CO_2 using vibrational spectroscopy.[25] They observed that the partial charge of nitrogen varied as a function of the substituent's Hammett parameter. However, they did not report the formation of carbamate bonds, likely due to the absence of a base in their system. Here, we study the aniline−CO_2 adducts in ambient temperature in the presence of an additional base and report the formation of a carbamate bond.

We also computationally explore the relationship between measurable carbamate frequencies and the Hammett parameter of the attached substituents to understand the underlying factors that control changes in frequency and reaction energy, along similar lines to recent studies by us and others.[26−30] Further, we create linear free energy relationships (LFERs) to guide the selection of *para*-substituents for aniline. Such linear relationships[31,32] connecting reaction rates or selectivity and the Hammett parameter of substituents have been developed to understand reactions relevant to CO_2 capture.[33,34] More recently, Zhang et al. have studied the suitability of alkoxides, phenoxides, and amines and developed an inverse design procedure for direct air capture of CO_2.[27]

In this work, we present experimental evidence of the formation of an adduct between a *para*-substituted aniline anion and CO_2 and report a peak in the FTIR spectrum associated with the asymmetric CO_2 carbamate stretch. The frequency of this stretch depends on the substituent's electron-donating/withdrawing ability as this governs the extent of charge transfer from the aniline anion to bound CO_2 in the carbamate, with electron-donating groups (EDGs) yielding lower or red-shifted frequencies relative to unsubstituted aniline. Energies of carbamate formation also depend on substituent electron-donating/withdrawing ability and are found to be strongly correlated to computationally determined IR frequencies. These similarities in frequency and reaction energy trends with respect to σ_p can serve as valuable means to track reaction energetics via easily observable spectroscopic features.

METHODS

Experimental Carbamate Formation and Characterization. All chemicals were purchased from MilliporeSigma and used as received. As some aniline derivatives were solid at room temperature, two different methods were used to create aniline−triethylamine (TEA) solutions. For solid anilines, a 5 mL saturated aniline−TEA solution was prepared, filtered using a syringe filter, and diluted with 1 mL of excess TEA. Liquid anilines were dissolved in a 1:2 mole ratio of TEA without further preparation. To induce carbamate formation, a pure CO_2 gas feed was bubbled into 10 mL vials containing the aniline−TEA solution.

For deuteration experiments, a 1:10 mole ratio solution of aniline in deuterated methanol (CH_3OD) was prepared. These solutions were left undisturbed for 2 days, and the methanol was removed using a RotaVap. After deuteration, aniline−TEA solutions were prepared as described above. Several of the carbamate complexes were viscous solutions.

All vibrational spectra were obtained using a Nicolet iS50 FT-IR under purge. The carbamate complexes were placed between two CaF_2 windows. The amount of carbamate sample was adjusted to ensure reasonable absorption spectra in the carbamate frequency region. The spectra were measured in a single-beam transmission configuration using a DTGS detector, with 400−4000 cm^{-1} range and 0.1 cm^{-1} resolution.

The FTIR spectra were transformed into absorbance, and a linear baseline was subtracted. The region between 1550 and 1710 cm^{-1} were fitted to a series of Lorentzians using Matlab's default curve fitting module and trust-region reflective algorithm. Additional details on the fits are provided in Supporting Information (SI) Section S2. Although we tried to dissolve the carbamates in various solvents, rapid degradation of the product back into aniline and TEA was observed. The full list of solvents tried is available in SI Section S3.

Computational Characterization of Carbamate Bond Formation. All calculations were performed using the *ab initio* quantum chemical software ver. Q-Chem 5.4.2.[35] We modeled 23 *para*- substituted anilines to explore possible correlations between the Hammett parameter, reactions energies, and the carbamate vibrational frequency. Optimized geometries for the carbamate product (final state, FS) were identified using density functional theory (DFT) calculations at the ωB97X-D/def2-TZVP level of theory.[36,37] The conductor-like polarizable continuum model (C-PCM) for implicit solvation[38−40] was used for all electronic structure calculations with dichloromethane (dielectric constant = 8.93) as the representative solvent. Dichloromethane was selected due to its dielectric

https://doi.org/10.1021/acs.jpca.3c01406
J. Phys. Chem. A 2023, 127, 5162−5170

constant being similar to that of ionic liquids, which approximates the carbamate$^-$−TEAH$^+$ product.[41] The carbamate frequency (ν_3) was identified for all products and adjusted by a scaling factor of 0.955 consistent with NIST scaling recommendations[42] (SI Section S4).

The initial state (IS) geometries, composed of weakly interacting complexes of deprotonated, substituted anilines and neutral CO_2, were calculated using constrained density functional theory (CDFT)[43−45] with unshifted Becke partitioning.[46] CDFT constrains the charge distribution such that the substituted aniline has one excess electron. Vibrational analysis was used to confirm that the geometries were minima. We approximated the free energy of formation of carbamate (difference between FS and IS) as the zero-point-corrected electronic energy difference between the two geometries (SI Section S5). This is because vibrational analysis yielded 1−3 small imaginary modes (≤100 cm^{-1}) for some of these structures, which are difficult to eliminate. Estimating free energy contributions from such modes can be challenging. These initial and final states were determined without the inclusion of TEA which would likely participate in hydrogen bonding with the bound CO_2. Including TEA in the model leads to shifts the ν_3 for some substituents (SI Section S4), but the overall trend with respect to the Hammett parameter is preserved. To further quantify the role of the amine, it will be necessary to scan the configurational space of hydrogen-bonding geometries and generate an ensemble description of reaction energies and corresponding vibrational frequencies, which is beyond the scope of this paper.

Using the computed formation energies and the characteristic carbamate frequencies (ν_3), we developed a simple LFER that allows one to predict the carbamate formation energy for a substituted aniline, ΔE_i, based on its calculated frequency, $\nu_{3,i}$:

$$\frac{\Delta E_i - \Delta E_{\mathrm{H}}}{RT} \approx m \times \frac{\nu_{3,i} - \nu_{3,\mathrm{H}}}{\nu_{3,\mathrm{MAX}} - \nu_{3,\mathrm{MIN}}} \quad (1)$$

Here, ΔE_{H} refers to the unsubstituted aniline, R is the gas constant, and T is the temperature. The right-hand side of eq 1 consists of frequencies of the unsubstituted aniline ($\nu_{3,\mathrm{H}}$) as well as maximum and minimum values of vibrational frequencies identified in our analysis of 23 substituted anilines and a unitless slope of linear fit, m. Note that our choice of normalization and the resulting slope depends on the range of frequencies within the data set. Referencing all reaction energies to ΔE_{H} helps prevent any changes in the trends stemming from our selection of the initial state for these systems.

The carbamate bond length between the nitrogen and carbon for every FS is also reported because bond lengths are often correlated to bond strength[47] (SI Section S4), although, as illustrated by Kraka and co-workers, caution is recommended in relating bond dissociation energy and bond length.[48,49] Similarly, we report the bond angle of bound CO_2 as a physical reflection of the extent of interaction between bound CO_2 and the substituted anilines (SI Section S4). Mulliken charges for carbon and nitrogen are reported for the FS and IS to explore the extent of charge transfer across the carbamate bond (SI Section S6). To better understand the dependence of bond strength on substituent and the subsequent shift in IR frequencies, we also performed natural bond orbital (NBO) analysis.[50−52] NBO analysis provides a measure of the occupancy of the bonding and antibonding orbitals between bound atoms. The occupancy of these orbitals was then shown to be related to the calculated frequencies as well as the calculated bond lengths (SI Section S6).

■ RESULTS AND DISCUSSION

Experimental Observation of Carbamate Formation. After bubbling CO_2 through the aniline−triethylamine (TEA) solution, we formed viscous products for most of the samples. This change in viscosity with CO_2 is the first indication of successful formation of carbamates as it suggests the formation of an ionic liquid between the carbamate and the protonated TEA. More details about the form of the products within the series are available in Table S3.

FTIR spectra of the other aniline derivatives under investigation are shown in SI Section S2. An example spectrum in the expected carbamate stretch frequency,[15,53] comparing the starting aniline solution to the product is shown in Figure 2, along with the identity of the most important spectral features for both species.

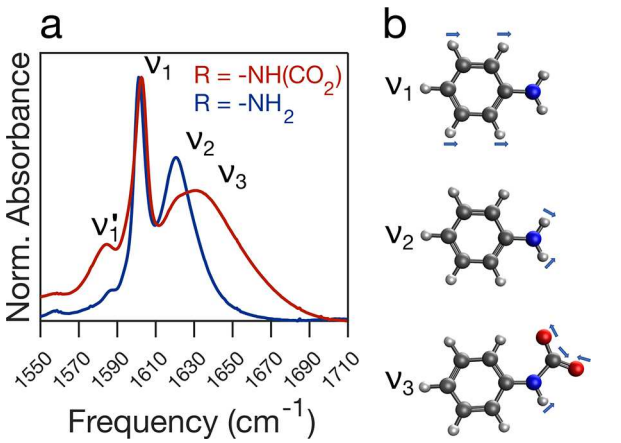

Figure 2. (a) FTIR spectra of aniline in triethylamine before (blue) and after (red) carbamate formation. (b) Identity of vibrational modes ν_1 (ν_1'), ν_2, and ν_3 as supported by computations.

Aniline (Figure 2, blue) displays a narrow peak (ν_1) at 1600 cm^{-1}, which is due to the characteristic carbon−carbon bond stretching of the aromatic ring.[14,16,19] There is an additional peak (ν_1') that is also assigned to an aromatic C═C stretch. In addition, there is a peak centered around 1630 cm^{-1} (ν_2) which we attribute to an amine bending mode based on computational results and their presence in other amine solutions (SI Section S2).[14,16,19]

Upon reaction with CO_2 (Figure 2, red), a new broader peak at 1640 cm^{-1} (ν_3) is formed. Our calculations for aniline−carbamate in this spectral region show a mode that primarily corresponds to the carbamate asymmetric stretch, suggesting the assignment of ν_3 to the carbamate bond. However, because of its overlap with ν_2 of aniline, the assignment of ν_3 to carbamate was less certain. To confirm the assignment, we performed the same experiments after deuterating the aniline amino group.

FTIR spectra taken after deuteration of the aniline−TEA solution are shown in Figure 3. As shown, deuteration largely removed the amino stretch from the initial solution (Figure 3a, blue). As the phenyl hydrogens were expected to be unaffected upon deuteration, ν_1 and ν_1' were unaffected. In contrast,ν_2 disappeared, leaving this area uncongested. Upon introduction

https://doi.org/10.1021/acs.jpca.3c01406
J. Phys. Chem. A 2023, 127, 5162−5170

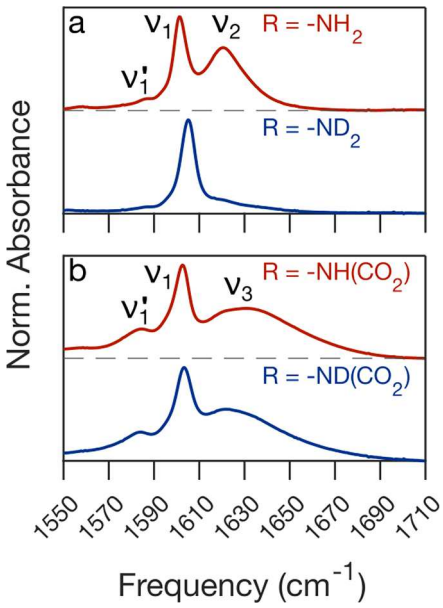

Figure 3. Example FTIR spectra showing the success of deuteration in isolating the carbamate stretching region from the amine stretching modes. (a) Comparison of nondeuterated aniline in triethylamine (TEA) to a deuterated sample. Upon deuteration, peaks associated with the NH_2 bending mode shift to lower energies, leaving the 1550−1700 cm^{-1} region uncongested. (b) Appearance on ν_3 in both deuterated and undeuterated sample, therefore confirming its assignment to the carbamate stretch.

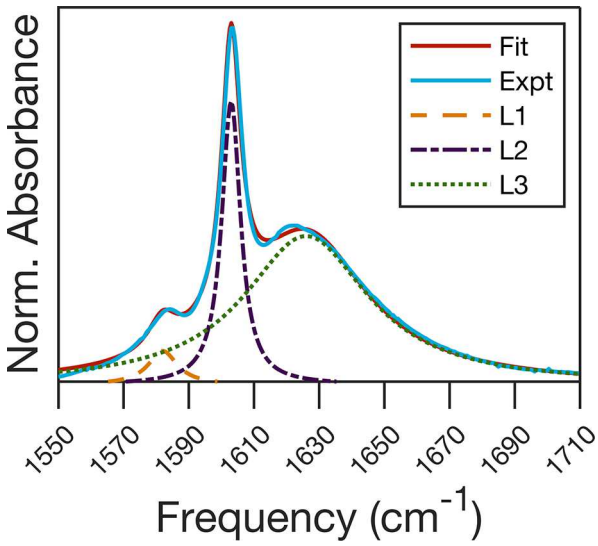

Figure 4. Representative spectrum of substituted aniline (R = −H) adducted with CO_2. The spectrum was fitted to three Lorentzian components as described in the text.

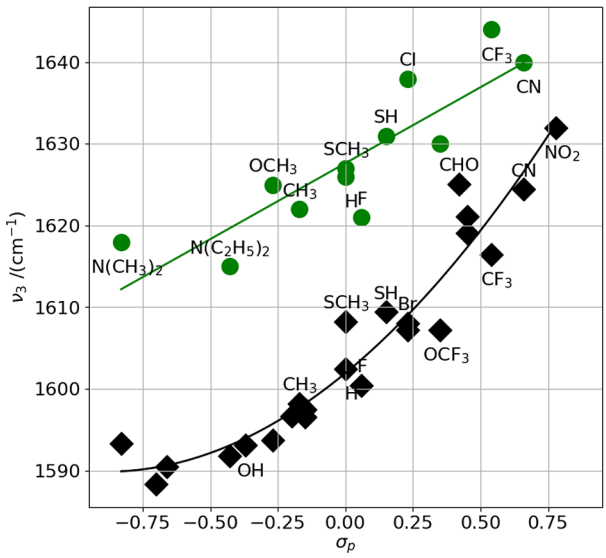

Figure 5. Comparison of trends in carbamate stretching frequency (ν_3) with varying Hammett parameter (σ_p) for *para*-substituted anilines. Both the experimental (green circles) and computational (black diamonds) frequencies show a blue-shift with increasing σ_p. The two data sets are fitted to linear (R^2 = 0.74) and quadratic (R^2 = 0.93) functions, respectively, based on the corrected Akaike information criterion (AICc) as explained in the text.

of CO_2 to the deuterated sample, a new peak (ν_3) emerged. As this peak is located in the same region for both deuterated and nondeuterated samples, this confirms its assignment to the carbamate stretch. (Figure 3b). In summary, deuteration selectively removes the amino stretch from the carbamate spectral range. Therefore, we used deuterated aniline for all subsequent experiments.

The formation of a broad peak around 2400 cm^{-1} was observed (Figure S2). Previous work done by Malohtra et al. assigns a similar feature to a strongly hydrogen-bonded N−H stretching mode in intramolecular hydrogen-bonding CO_2 capturing agents.[54] They also report a pronounced change in viscosity due to the Coulombic interactions between zwitterions upon carbamate formation.[54] In our case the hydrogen bonding is intermolecular, and it suggests the carbamate adduct is stabilized by a triethylammonium cation, which was not included in our DFT calculations. However, we expect that this stabilizing interaction is similar across our series and would not change the overall trend we observe.

To isolate the carbamate stretch, it was necessary to fit the spectra to at least three Lorentzians. An example fit for aniline carbamate is shown in Figure 4. All other fits and the fits parameters are shown in SI Section S2.

Dependence of Carbamate Frequency on Substituents. The carbamate central frequency (ν_3) as retrieved from the fits is plotted versus the Hammett parameter, σ_p, of the aniline substituent in Figure 5 (green circles). As the figure shows, the carbamate frequency blue-shifts with increasing Hammett parameter. Calculated ν_3 values also exhibit a similar trend with σ_p (black diamonds, Figure 5). The calculated ν_3 frequencies are on average 52 cm^{-1} higher than experimental frequencies before the scaling adjustment (as explained in the Methods section) and are on average 24 cm^{-1} lower after scaling (SI Section S4).[55] Note that the purpose of the computations is to identify the trend in frequency variation rather than the exact values.

The computed frequencies exhibited a relatively flat response as the substituents become more electron-donating; i.e., σ_p becomes more negative. This flattened response suggested fitting the computed frequencies to a quadratic form. To further justify this choice, the corrected Akaike information criterion (AICc) was employed to quantitatively describe the correlation between the calculated ν_3 and σ_p. AICc is a method for model selection based on a trade-off between the number of model parameters and goodness of the fit. We employed AICc to determine the polynomial orders that most

https://doi.org/10.1021/acs.jpca.3c01406
J. Phys. Chem. A 2023, 127, 5162−5170

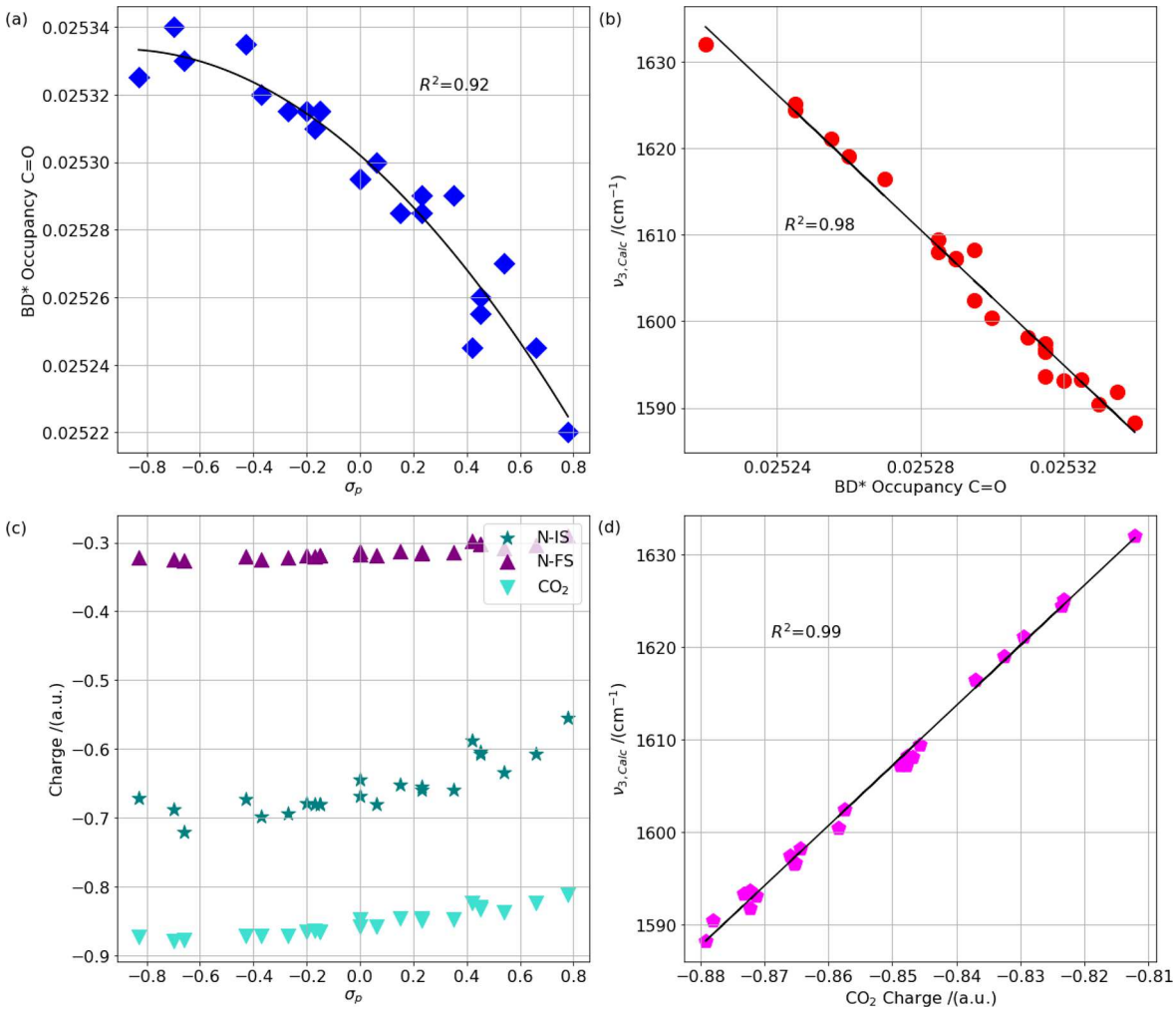

Figure 6. Results of NBO and Mulliken charge analysis. (a) Antibonding orbital occupancy (BD*) of the bond between carbon and oxygen (C═O) versus σ_p shows a quadratic relation as determined using AICc. (b) Calculated carbamate frequency (ν_3) versus C═O antibonding orbital occupancy show a linear correlation. (c) Mulliken charge of the nitrogen in the anionic aniline (IS, stars), of the nitrogen in the carbamate (FS, upward triangles), and of the CO_2 fragment in the carbamate (downward triangles) versus σ_p. (d) Calculated carbamate ν_3 frequency versus charge of the CO_2 fragment in carbamate showing a linear relation.

accurately described the calculated frequencies (SI Section S4). The method suggested a quadratic fit (R^2 = 0.93). The experimental data also suggest a similar flattening at negative σ_p, as seen in Figure 5. However, we did not have access to enough commercially available molecules to take more data points in that region. When the AICc method was applied to this data, a linear fit was suggested (R^2 = 0.74). While calculated ν_3 for the most electron-donating substituent ($N(CH_3)_2$) is slightly higher than its immediate predecessor ($NHCH_3$), more calculations with substituents of even higher electron-donating character, or possibly negatively charged substituents, are necessary before determining whether frequencies flatten or reach a minimum around $\sigma_p \approx -0.75$.

Computational Characterization of Carbamate Bond Strength. As the carbamate bond is formed, CO_2 accepts charge from the anionic aniline and adopts a bent structure. We determined the average Mulliken charge of bound CO_2 to be −0.853 (Figure 6d and SI Section S6). Upon partial charge transfer, the asymmetric vibration of free CO_2 in solution (2336 cm^{-1}) red-shifts by a large value (ν_3 = 1602 cm^{-1} for unsubstituted aniline−carbamate). This red-shift of the CO_2 asymmetric stretch has been ascribed to both electron donation into the antibonding orbital of the CO_2 fragment and to lessening of the mechanical coupling between the local mode C−O vibrations due to bending.[56]

The connection between the red-shift of CO_2's asymmetric stretch and the occupancy of the antibonding orbital on CO_2 suggests that tuning the electron-donating capability of the substituent on aniline should impact the antibonding occupancy. To explore this effect, we quantified the occupancy of the antibonding orbitals using the natural bond orbital (NBO) analysis. The occupancy of the antibonding orbital between the C and the O of the CO_2 fragment decreases with increasing σ_p (Figure 6a). This decreased occupancy of the antibonding orbital on CO_2 results in a stronger bond and therefore accounts for the blue-shift in ν_3 with increasing σ_p of the substituent. This occupancy correlates well with the computed frequency, as shown in Figure 6b. Note that both the antibonding occupancy of the carbon−oxygen bond in the CO_2 fragment and the frequency of its vibration (ν_3) vary quadratically with σ_p. Therefore, the occupancy and the frequency show a linear relation (R^2 = 0.98). These characteristics are also reflected in the Mulliken charges reported in Figure 6c,d. The nitrogen charge upon adduct

https://doi.org/10.1021/acs.jpca.3c01406
J. Phys. Chem. A 2023, 127, 5162−5170

formation becomes less negative, implying partial electron transfer to CO_2 (Figure 6c). Note that charge in the initial state, IS (aniline anion), is more sensitive to the substituent's σ_p compared to the final state, FS (aniline−carbamate). Thus, the extent of charge transfer decreases with increasing σ_p. A corresponding trend is observed for the CO_2 fragment. Given these relationships, the CO_2 partial charge linearly correlates with the frequency for ν_3 (Figure 6d, R^2 = 0.99).

Both C−N bond length and bound CO_2 bond angle are linearly correlated to ν_3 (R^2 = 0.99 for both, SI Section S4) and are geometrical manifestations of the partial charge transfer from the substituted anilines to bound CO_2. We have also performed NBO analysis for the C−N bond in carbamate (SI Section S6) and have observed behavior that is consistent with the picture presented above.

Predicting the Driving Force for Carbamate Formation. One important outcome of our work is that the computed ν_3 is linearly correlated to the computed zero-point-corrected reaction energy of carbamate bond formation for substituted anilines. As outlined in eq 1, we constructed a dimensionless linear free energy relation (LFER) using the 23 carbamates examined computationally. Figure 7 shows the relation between the scaled energies and the scaled frequencies, resulting in a slope of m = 27.6.

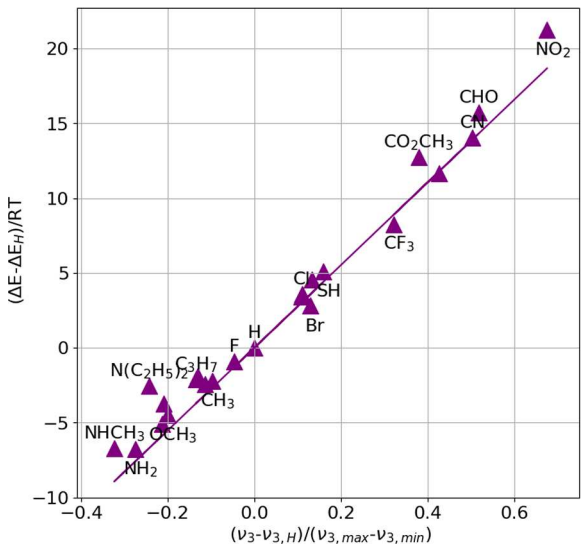

Figure 7. Relation between carbamate formation energies and calculated carbamate frequencies. Both quantities are scaled relative to unsubstituted aniline, as described in the text.

The figure shows that electron-donating groups (EDGs) lead to more spontaneous carbamate formation. EDGs destabilize the aniline anion's highest occupied molecular orbital (HOMO), providing an increased driving force for carbamate formation as shown in SI Section S5.

Because the experimental frequencies correlate reasonably with the computed frequencies (Figure S3, R^2 = 0.77), the above approach has the potential to estimate the relative reaction energies based on observation of the experimental carbamate frequencies (Figure S6). Note that for computations an implicit solvation model was used. To obtain better correlation between the experimental and computational frequencies, it will be necessary to include explicit solvents, account for the interaction of the protonated base with the adduct, and include possible interaction between adducts. Future efforts may focus on these issues.

Our computations show that carbamate reaction energy is strongly correlated to the ν_3 frequency of the asymmetric carbamate stretch. This correlation could prove invaluable because it has the potential to connect a convenient spectroscopic observable, i.e., the carbamate ν_3 frequency, to the often difficult to measure reaction energy. Even though successful techniques have been developed for gas phase calorimetry measurements on surfaces, condensed phase experiments remain challenging.[57,58] Such an easily observable spectroscopic measure could help identify trends in reaction energetics even when direct calorimetry is difficult. It is also likely that similar connections between reaction energies and the analogous asymmetric CO_2 stretch can extend to other chemical capture systems.

Previous work by some of us observed that a polarizing electrode exerts a similar effect to that of a polarizing functional group.[22] Therefore, it is plausible that the reaction energy for CO_2 adsorption to an electrode-bound aniline will also display a similar dependence on the potential. In that case, the frequency−energy map in Figure 7 will serve as an important handle to understand the electroadsorption energy and will ease experimental difficulties in determining energetics, particularly for surfaces. Furthermore, this idea can be extended such that the polarizing effect of the electrode could be used for reversible CO_2 capture.

We noted that these reactions produce a viscous material, which likely impacts the system's CO_2 absorption kinetics and holding capacity. The influence of this phase change and the physical properties of the carbamate and the associated protonated base need to be studied in further detail. Such phase changes may make experimental measurement of the equilibrium constants and consequently the reaction energy difficult. Verification of the reaction energies by calorimetry or by observation of the temperature-dependent equilibrium constant would provide further experimental tests of the relations established in this study. In fact, exploring the full phase diagram of the stability of the complex as a function of temperature, partial pressure of CO_2, and loading of the base, similar to the work done on alkylamines, might prove fruitful.[18,25]

We observed that the adducts were extremely sensitive to solvents. Therefore, the solvent properties, such as the dielectric constant, may also affect the stability of the anionic carbamate and the corresponding cationic protonated base. Although there has been numerous computational and experimental works on the reaction mechanisms behind CO_2 capture using amine systems,[16,18,19,53,59−68] advanced spectroscopic approaches, such as 2DIR and time-resolved measurements, could help reveal plausible reaction mechanisms. The mechanistic details of carbamate formation are still ambiguous as the reaction potentially requires or is stabilized by the interaction of solvent, one or more base molecules, aniline, and CO_2. It is plausible that deprotonation and carbamate bond formation may occur in a single concerted step. Solvent environment could be very important in CO_2 capture systems and change the strength and the selectivity of the CO_2 capture.[69] It might be beneficial to further investigate the effects of the solvent on the capture mechanisms.

https://doi.org/10.1021/acs.jpca.3c01406
J. Phys. Chem. A 2023, 127, 5162−5170

CONCLUSIONS

We reported that the vibrational frequency of the asymmetric stretch of an aniline−carbamate is correlated to the Hammett parameter of the attached *para*-substituents. The carbamate bond forms by donation of electron density from the aniline to the CO_2 antibonding orbitals, which results in a red-shift of the asymmetric stretch. The substituent's electron-donating capability controls the extent of this charge transfer. Therefore, both the frequency of the carbamate and the energy of the reaction are affected by the substituent. The resulting reaction energy is linearly correlated to the computed frequency.

We caution against directly applying our LFER or comparing our reaction energies to the more ubiquitous alkylamines used for CO_2 capture. This is because aniline is more polarizable than alkylamines due to the electron-rich phenyl group. As such, we can more easily modify the partial charge transfer from nitrogen to CO_2 through substitutions to aniline compared to alkylamines. This means the slope of our LFER is unlikely to directly apply to nonconjugated amines like monoethanolamine. For the reaction energies, we ignore specific interactions between the primary carbamate and neighboring molecules. Although we expect these interactions to be similar across our experimental data set, solvent effects will determine the precise energetic drive for carbamate formation and should be considered when comparing different amine−CO_2 systems.[20,68,70] We also did not study the effect of crowding on the amine nitrogen or hydrogen bonding between the amine and surrounding hydrogen-bond donors, which are both important factors.[16,54,67,68] Despite this caveat, our computed reaction energies, which vary between approximately −160 and −80 kJ/mol, are within a factor of 2 of the general range found for aqueous alkylamine CO_2 capture systems.[20] A precise calorimetric study on the derived aniline−CO_2 adduct is necessary before we can definitively say whether our aniline systems are in the same energy range of other carbamate systems. However, their comparatively worse stability to a low CO_2 environment suggests aniline has a smaller free energy driving force toward carbamate formation compared to other amine systems. Their seemingly weaker CO_2 bond and their tunability combined suggest anilines are a promising platform for deriving next-generation reversible amine CO_2 capture systems.

The correlation between the asymmetric CO_2 stretching frequency and its formation energy is driven largely by changes within the CO_2 fragment. Thus, we expect analogous trends in other amine−CO_2 capture systems. The value of our study is in the fact that measuring a vibrational spectrum is often easier and more accessible than calorimetry, especially in complex environments. This work also naturally extends to electrodes decorated with aniline for reversible non-Faradaic electrochemical CO_2 capture. Additionally, this work may prove useful for understanding photoinduced CO_2 reduction using organic molecular initiators, such as oligo-*para*-phenylenes studied by us previously.[71]

ASSOCIATED CONTENT

Supporting Information

The Supporting Information is available free of charge at https://pubs.acs.org/doi/10.1021/acs.jpca.3c01406.

Deuterated aniline FTIR spectra before and after carbamate formation, summary tables and visualization of fits to deuterated aniline−carbamate spectra, descriptions of experimentally formed products, complete data for all discussed computational results with additional figures for ease of data visualization, and the *XYZ* coordinates of predicted geometries for the initial state (IS) and final state (FS) (PDF)

AUTHOR INFORMATION

Corresponding Authors

Shaama Mallikarjun Sharada − *Mork Family Department of Chemical Engineering and Materials Science, University of Southern California, Los Angeles, California 90089, United States; Department of Chemistry, University of Southern California, Los Angeles, California 90089, United States;* orcid.org/0000-0001-7332-5373; Email: ssharada@usc.edu

Jahan M. Dawlaty − *Department of Chemistry, University of Southern California, Los Angeles, California 90089, United States;* orcid.org/0000-0001-5218-847X; Email: dawlaty@usc.edu

Authors

Berk Delibas − *Department of Chemistry, University of Southern California, Los Angeles, California 90089, United States*

Kareesa J. Kron − *Mork Family Department of Chemical Engineering and Materials Science, University of Southern California, Los Angeles, California 90089, United States;* orcid.org/0000-0001-9057-6211

Daniel E. Cotton − *Department of Chemistry, University of Southern California, Los Angeles, California 90089, United States;* orcid.org/0000-0002-5170-7108

Noemi Salazar − *Department of Chemistry, University of Southern California, Los Angeles, California 90089, United States*

Complete contact information is available at: https://pubs.acs.org/10.1021/acs.jpca.3c01406

Notes

The authors declare no competing financial interest.

ACKNOWLEDGMENTS

J.M.D., D.E.C., B.D., and N.S. were supported under Grant DE-SC0022173 from the Department of Energy (DOE) and Grant CHE 2154493 from the National Science Foundation (NSF). K.J.K. and S.M.S. were supported by the National Science Foundation under Grant 2102044 and Scialog: Negative Emissions Science (NES Award No. 27700) by the Research Corporation for Science Advancement. The authors acknowledge computational resources and support provided by the Collaboratory for Advanced Research Computing at USC. We thank Diego Pablo Montaño Velazquez from Valery Fokin's group at USC for access to their rotary evaporator.

REFERENCES

(1) Shukla, P. R.; Skea, J.; Reisinger, A.; Slade, R.; Fradera, R.; Pathak, M.; Al Khourdajie, A.; Belkacemi, M.; van Diemen, R.; Hasija, A.; et al. Contribution of Working Group III to the Sixth Assessment Report of the Intergovernmental Panel on Climate Change. *IPCC* **2022**.

(2) Rheinhardt, J. H.; Singh, P.; Tarakeshwar, P.; Buttry, D. A. Electrochemical Capture and Release of Carbon Dioxide. *ACS Energy Lett.* **2017**, *2*, 454−461.

(3) Sharifian, R.; Wagterveld, R. M.; Digdaya, I. A.; Xiang, C.; Vermaas, D. A. Electrochemical carbon dioxide capture to close the carbon cycle. *Energy Environ. Sci.* **2021**, *14*, 781−814.
(4) Zhang, H.; Zhang, Y.; Li, Y.; Ahn, S.; Palmore, G. T. R.; Fu, J.; Peterson, A. A.; Sun, S. Cu nanowire-catalyzed electrochemical reduction of CO or CO_2. *Nanoscale* **2019**, *11*, 12075−12079.
(5) McDaniel, J. G.; Yu, K.; Schmidt, J. R. Ab Initio, Physically Motivated Force Fields for CO_2 Adsorption in Zeolitic Imidazolate Frameworks. *J. Phys. Chem. C* **2012**, *116*, 1892−1903.
(6) Osman, A. I.; Hefny, M.; Abdel Maksoud, M. I. A.; Elgarahy, A. M.; Rooney, D. W. Recent advances in carbon capture storage and utilisation technologies: a review. *Environ. Chem. Lett.* **2021**, *19*, 797−849.
(7) Kazemifar, F. A review of technologies for carbon capture, sequestration, and utilization: Cost, capacity, and technology readiness. *Greenh. Gases* **2022**, *12*, 200−230.
(8) Romanov, V.; Soong, Y.; Carney, C.; Rush, G. E.; Nielsen, B.; O'Connor, W. Mineralization of Carbon Dioxide: A Literature Review. *ChemBioEng. Rev.* **2015**, *2*, 231−256.
(9) Snæbjörnsdóttir, S. Ó.; Sigfússon, B.; Marieni, C.; Goldberg, D.; Gislason, S. R.; Oelkers, E. H. Carbon dioxide storage through mineral carbonation. *Nat. Rev. Earth Environ.* **2020**, *1*, 90−102.
(10) Wang, W.; Hu, M.; Zheng, Y.; Wang, P.; Ma, C. CO_2 Fixation in Ca2+-/Mg2+-Rich Aqueous Solutions through Enhanced Carbonate Precipitation. *Ind. Eng. Chem. Res.* **2011**, *50*, 8333−8339.
(11) Gurkan, B.; Su, X.; Klemm, A.; Kim, Y.; Sharada, S. M.; Rodriguez-Katakura, A.; Kron, K. J. Perspective and challenges in electrochemical approaches for reactive CO_2 separations. *iScience* **2021**, *24*, 103422.
(12) Bui, M.; Adjiman, C. S.; Bardow, A.; Anthony, E. J.; Boston, A.; Brown, S.; Fennell, P. S.; Fuss, S.; Galindo, A.; Hackett, L. A.; et al. Carbon capture and storage (CCS): the way forward. *Energy Environ. Sci.* **2018**, *11*, 1062−1176.
(13) Rochelle, G. T. Amine Scrubbing for CO_2 Capture. *Science* **2009**, *325*, 1652−1654.
(14) Jackson, P.; Robinson, K.; Puxty, G.; Attalla, M. In situ Fourier Transform-Infrared (FT-IR) analysis of carbon dioxide absorption and desorption in amine solutions. *Energy Procedia* **2009**, *1*, 985−994.
(15) Sun, C.; Dutta, P. K. Infrared Spectroscopic Study of Reaction of Carbon Dioxide with Aqueous Monoethanolamine Solutions. *Ind. Eng. Chem. Res.* **2016**, *55*, 6276−6283.
(16) Robinson, K.; McCluskey, A.; Attalla, M. I. An FTIR Spectroscopic Study on the Effect of Molecular Structural Variations on the CO_2 Absorption Characteristics of Heterocyclic Amines. *ChemPhysChem* **2011**, *12*, 1088−1099.
(17) Li, X.; Zhao, X.; Liu, Y.; Hatton, T. A.; Liu, Y. Redox-tunable Lewis bases for electrochemical carbon dioxide capture. *Nat. Energy* **2022**, *7*, 1065−1075.
(18) Mannisto, J. K.; Pavlovic, L.; Tiainen, T.; Nieger, M.; Sahari, A.; Hopmann, K. H.; Repo, T. Mechanistic insights into carbamate formation from CO_2 and amines: the role of guanidine−CO_2 adducts. *Catal. Sci. Technol.* **2021**, *11*, 6877−6886.
(19) Robinson, K.; McCluskey, A.; Attalla, M. I. An ATR-FTIR Study on the Effect of Molecular Structural Variations on the CO_2 Absorption Characteristics of Heterocyclic Amines, Part II. *ChemPhysChem* **2012**, *13*, 2331−2341.
(20) Jerng, S. E.; Gallant, B. M. Electrochemical reduction of CO_2 in the captured state using aqueous or nonaqueous amines. *iScience* **2022**, *25*, 104558.
(21) Hansch, C.; Leo, A.; Taft, R. W. A survey of Hammett substituent constants and resonance and field parameters. *Chem. Rev.* **1991**, *91*, 165−195.
(22) Sarkar, S.; Patrow, J. G.; Voegtle, M. J.; Pennathur, A. K.; Dawlaty, J. M. Electrodes as Polarizing Functional Groups: Correlation between Hammett Parameters and Electrochemical Polarization. *J. Phys. Chem. C* **2019**, *123*, 4926−4937.
(23) Hammett, L. P. The Effect of Structure upon the Reactions of Organic Compounds. Benzene Derivatives. *J. Am. Chem. Soc.* **1937**, *59*, 96−103.
(24) Fernández, I.; Frenking, G. Correlation between Hammett Substituent Constants and Directly Calculated π-Conjugation Strength. *J. Org. Chem.* **2006**, *71*, 2251−2256.
(25) Farbos, B.; Tassaing, T. Substituent effect on the interaction of aromatic primary amines and diamines with supercritical CO_2 from infrared spectroscopy and quantum calculations. *Phys. Chem. Chem. Phys.* **2009**, *11*, 5052−5061.
(26) Kron, K. J.; Gomez, S. J.; Mao, Y.; Cave, R. J.; Mallikarjun Sharada, S. Computational Analysis of Electron Transfer Kinetics for CO_2 Reduction with Organic Photoredox Catalysts. *J. Phys. Chem. A* **2020**, *124*, 5359−5368.
(27) Zhang, Z.; Kummeth, A. L.; Yang, Y.; Alexandrova, A. N. Inverse molecular design of alkoxides and phenoxides for aqueous direct air capture of CO_2. *Proc. Natl. Acad. Sci. U. S. A.* **2022**, *119*, No. e2123496119.
(28) Siegel, J. B.; Zanghellini, A.; Lovick, H. M.; Kiss, G.; Lambert, A. R.; St. Clair, J. L.; Gallaher, J. L.; Hilvert, D.; Gelb, M. H.; Stoddard, B. L.; Houk, K. N.; Michael, F. E.; Baker, D. Computational design of an enzyme catalyst for a stereoselective bimolecular Diels-Alder reaction. *Science* **2010**, *329*, 309−313.
(29) Wheeler, S. E. Understanding substituent effects in noncovalent interactions involving aromatic rings. *Acc. Chem. Res.* **2013**, *46*, 1029−1038.
(30) Prampolini, G.; Bellina, F.; Biczysko, M.; Cappelli, C.; Carta, L.; Lessi, M.; Pucci, A.; Ruggeri, G.; Barone, V. Computational Design, Synthesis, and Mechanochromic Properties of New Thiophene-Based -Conjugated Chromophores. *Chem.—Eur. J.* **2013**, *19*, 1996−2004.
(31) Burello, E.; Rothenberg, G. In silico design in homogeneous catalysis using descriptor modelling. *Int. J. Mol. Sci.* **2006**, *7*, 375−404.
(32) Durand, D. J.; Fey, N. Computational Ligand Descriptors for Catalyst Design. *Chem. Rev.* **2019**, *119*, 6561−6594.
(33) Barlow, J. M.; Yang, J. Y. Oxygen-Stable Electrochemical CO_2Capture and Concentration with Quinones Using Alcohol Additives. *J. Am. Chem. Soc.* **2022**, *144*, 14161−14169.
(34) Oktavian, R.; Taha, M.; Lee, M. J. Experimental and computational study of CO_2 storage and sequestration with aqueous 2-amino-2-hydroxymethyl-1,3-propanediol (TRIS) solutions. *J. Phys. Chem. A* **2014**, *118*, 11572−11582.
(35) Epifanovsky, E.; Gilbert, A. T. B.; Feng, X.; Lee, J.; Mao, Y.; Mardirossian, N.; Pokhilko, P.; White, A. F.; Coons, M. P.; Dempwolff, A. L.; et al. Software for the frontiers of quantum chemistry: An overview of developments in the Q-Chem 5 package. *J. Chem. Phys.* **2021**, *155*, 084801.
(36) Chai, J.-D.; Head-Gordon, M. Long-range corrected hybrid density functionals with damped atom-atom dispersion corrections. *Phys. Chem. Chem. Phys.* **2008**, *10*, 6615−6620.
(37) Chai, J.-D.; Head-Gordon, M. Systematic optimization of long-range corrected hybrid density functionals. *J. Chem. Phys.* **2008**, *128*, 084106.
(38) Truong, T. N.; Stefanovich, E. V. A new method for incorporating solvent effect into the classical, ab initio molecular orbital and density functional theory frameworks for arbitrary shape cavity. *Chem. Phys. Lett.* **1995**, *240*, 253−260.
(39) Barone, V.; Cossi, M. Quantum Calculation of Molecular Energies and Energy Gradients in Solution by a Conductor Solvent Model. *J. Phys. Chem. A* **1998**, *102*, 1995−2001.
(40) Cossi, M.; Rega, N.; Scalmani, G.; Barone, V. Energies, structures, and electronic properties of molecules in solution with the C-PCM solvation model. *J. Comput. Chem.* **2003**, *24*, 669−681.
(41) Weingärtner, H. The Static Dielectric Constant of Ionic Liquids. *Z. Phys. Chem.* **2006**, *220*, 1395−1405.
(42) Precomputed vibrational scaling factors, 2022; https://cccbdb.nist.gov/.
(43) Wu, Q.; Van Voorhis, T. Direct optimization method to study constrained systems within density-functional theory. *Phys. Rev. A* **2005**, *72*, 024502.
(44) Wu, Q.; Van Voorhis, T. Direct calculation of electron transfer parameters through constrained density functional theory. *J. Phys. Chem. A* **2006**, *110*, 9212−9218.

https://doi.org/10.1021/acs.jpca.3c01406
J. Phys. Chem. A 2023, 127, 5162−5170

(45) Kaduk, B.; Kowalczyk, T.; Van Voorhis, T. Constrained density functional theory. *Chem. Rev.* **2012**, *112*, 321−370.
(46) Becke, A. D. A multicenter numerical integration scheme for polyatomic molecules. *J. Chem. Phys.* **1988**, *88*, 2547−2553.
(47) Badger, R. M. The Relation Between the Internuclear Distances and Force Constants of Molecules and Its Application to Polyatomic Molecules. *J. Chem. Phys.* **1935**, *3*, 710−714.
(48) Kraka, E.; Setiawan, D.; Cremer, D. Re-evaluation of the bond length−bond strength rule: The stronger bond is not always the shorter bond. *J. Comput. Chem.* **2016**, *37*, 130−142.
(49) Cremer, D.; Wu, A.; Larsson, A.; Kraka, E. Some Thoughts about Bond Energies, Bond Lengths, and Force Constants. *Mol. Model. Annu.* **2000**, *6*, 396−412.
(50) Weinhold, F.; Landis, C.; Glendening, E. What is NBO analysis and how is it useful? *Int. Rev. Phys. Chem.* **2016**, *35*, 399−440.
(51) Reed, A. E.; Curtiss, L. A.; Weinhold, F. Intermolecular Interactions from a Natural Bond Orbital, Donor—Acceptor Viewpoint. *Chem. Rev.* **1988**, *88*, 899−926.
(52) Glendening, E. D.; Landis, C. R.; Weinhold, F. Natural bond orbital methods. *Wiley Interdiscip. Rev. Comput. Mol. Sci.* **2012**, *2*, 1−42.
(53) du Preez, L. J.; Motang, N.; Callanan, L. H.; Burger, A. J. Determining the Liquid Phase Equilibrium Speciation of the CO_2−MEA−H_2O System Using a Simplified in Situ Fourier Transform Infrared Method. *Ind. Eng. Chem. Res.* **2019**, *58*, 469−478.
(54) Malhotra, D.; Cantu, D. C.; Koech, P. K.; Heldebrant, D. J.; Karkamkar, A.; Zheng, F.; Bearden, M. D.; Rousseau, R.; Glezakou, V.-A. Directed Hydrogen Bond Placement: Low Viscosity Amine Solvents for CO_2 Capture. *ACS Sustain. Chem. Eng.* **2019**, *7*, 7535−7542.
(55) Alecu, I.; Zheng, J.; Zhao, Y.; Truhlar, D. G. Computational thermochemistry: scale factor databases and scale factors for vibrational frequencies obtained from electronic model chemistries. *J. Chem. Theory Comput.* **2010**, *6*, 2872−2887.
(56) Dodson, L. G.; Thompson, M. C.; Weber, J. M. Characterization of Intermediate Oxidation States in CO_2 Activation. *Annu. Rev. Phys. Chem.* **2018**, *69*, 231−252.
(57) Silbaugh, T. L.; Campbell, C. T. Energies of Formation Reactions Measured for Adsorbates on Late Transition Metal Surfaces. *J. Phys. Chem. C* **2016**, *120*, 25161−25172.
(58) Fubini, B. Adsorption calorimetry in surface chemistry. *Thermochim. Acta* **1988**, *135*, 19−29.
(59) Carpenter, B. K. Computational study of CO_2 reduction by amines. *J. Phys. Chem. A* **2007**, *111*, 3719−3726.
(60) Mao, Y.; Loipersberger, M.; Kron, K. J.; Derrick, J. S.; Chang, C. J.; Sharada, S. M.; Head-Gordon, M. Consistent inclusion of continuum solvation in energy decomposition analysis: theory and application to molecular CO_2 reduction catalysts. *Chem. Sci.* **2021**, *12*, 1398−1414.
(61) Crooks, J. E.; Donnellan, J. P. Kinetics and mechanism of the reaction between carbon dioxide and amines in aqueous solution. *J. Chem. Soc., Perkin Trans.* **1989**, *2*, 331.
(62) Xiao, M.; Liu, H.; Idem, R.; Tontiwachwuthikul, P.; Liang, Z. A study of structure−activity relationships of commercial tertiary amines for post-combustion CO_2 capture. *Appl. Energy* **2016**, *184*, 219−229.
(63) Nakai, H.; Nishimura, Y.; Kaiho, T.; Kubota, T.; Sato, H. Contrasting mechanisms for CO_2 absorption and regeneration processes in aqueous amine solutions: Insights from density-functional tight-binding molecular dynamics simulations. *Chem. Phys. Lett.* **2016**, *647*, 127−131.
(64) Xie, H.-B.; He, N.; Song, Z.; Chen, J.; Li, X. Theoretical Investigation on the Different Reaction Mechanisms of Aqueous 2-Amino-2-methyl-1-propanol and Monoethanolamine with CO_2. *Ind. Eng. Chem. Res.* **2014**, *53*, 3363−3372.
(65) Pate, S. G.; Xu, H.; O'Brien, C. P. Operando observation of CO_2 transport intermediates in polyvinylamine facilitated transport membranes, and the role of water in the formation of intermediates, using transmission FTIR spectroscopy. *J. Mater. Chem. A* **2022**, *10*, 4418−4427.
(66) Sumon, K. Z.; Henni, A.; East, A. L. L. Molecular Dynamics Simulations of Proposed Intermediates in the CO_2 + Aqueous Amine Reaction. *J. Phys. Chem. Lett.* **2014**, *5*, 1151−1156.
(67) Stowe, H. M.; Vilčiauskas, L.; Paek, E.; Hwang, G. S. On the origin of preferred bicarbonate production from carbon dioxide (CO_2) capture in aqueous 2-amino-2-methyl-1-propanol (AMP). *Phys. Chem. Chem. Phys.* **2015**, *17*, 29184−29192.
(68) Ma, C.; Pietrucci, F.; Andreoni, W. Capturing CO_2 in Monoethanolamine (MEA) Aqueous Solutions: Fingerprints of Carbamate Formation Assessed with First-Principles Simulations. *J. Phys. Chem. Lett.* **2014**, *5*, 1672−1677.
(69) Kash, B. C.; Gomes, R. J.; Amanchukwu, C. V. Mitigating Electrode Inactivation during CO_2 Electrocatalysis in Aprotic Solvents with Alkali Cations. *J. Phys. Chem. Lett.* **2023**, *14*, 920−926.
(70) Lv, B.; Guo, B.; Zhou, Z.; Jing, G. Mechanisms of CO_2 Capture into Monoethanolamine Solution with Different CO_2 Loading during the Absorption/Desorption Processes. *Environ. Sci. Technol.* **2015**, *49*, 10728−10735.
(71) Kron, K. J.; Hunt, J. R.; Dawlaty, J. M.; Mallikarjun Sharada, S. Modeling and Characterization of Exciplexes in Photoredox CO_2 Reduction: Insights from Quantum Chemistry and Fluorescence Spectroscopy. *J. Phys. Chem. A* **2022**, *126*, 2319−2329.

https://doi.org/10.1021/acs.jpca.3c01406
J. Phys. Chem. A 2023, 127, 5162−5170